THE AMERICAN SOCIETY OF MECHANICAL ENGINEERS
345 E. 47 St., New York, N.Y. 10017

91-GT-110

Stability and Instability of a Two-Mode Rotor Supported by Two Fluid-Lubricated Bearings

AGNES MUSZYNSKA, JOHN W. GRANT
Bently Rotor Dynamics Research Corporation
Minden, Nevada

ABSTRACT

This paper is a continuation of the series of papers on application of the improved fluid force model for lightly loaded shafts rotating in a fluid environment. The fluid force model is based on the strength of the circumferential flow. The considered two—mode rotor is supported in two fluid—lubricated bearings, thus it contains two potential sources of instability. The eigenvalue solution predicts thresholds of stability and provide natural frequencies and modes of the system, including the flow—induced modes The nonlinear model of the rotor/bearing system allows for evaluation of parameters of after instability onset self—excited vibrations (whirl and whip). Experimental data illustrate the dynamic phenomena predicted by the model. In particular, they show an undocumented new phenomenon, the simultaneous existence of two whip vibrations with frequencies corresponding to two modes of the rotor. A radial preload of the rotor results in specific changes of the fluid forces (an increase of radial stiffness and reduction of circumferential velocity) providing better stability of the rotor. This effect predicted by the model is illustrated by the experimental data.

NOMENCLATURE

$A_1,...,A_4$	Amplitudes of rotor lateral self-excited vibrations
D_1,D_2	Bearing fluid film radial damping coefficients
D_{S1},D_{S2}	Rotor modal damping coefficients
i,ν	Integers
$j=\sqrt{-1}$	
$K_1,...,K_8$	Rotor modal stiffnesses (coupled two-mode rotor)
K_{B1},K_{B2}	Bearing fluid film radial stiffnesses
$M_1,...,M_4$	Rotor modal masses
$s=j\omega$	Eigenvalue
x_i,y_i	Rotor horizontal and vertical displacements respectively
$z_1,...,z_5$	Rotor lateral displacements
$\alpha_1,\alpha_2,\alpha_3$	Phases of rotor lateral self-excited vibrations
$\beta_{i\nu}$	Modal function phase angles
$\kappa_1,...,\kappa_4$	Complex dynamic stiffnesses of the rotor system (Eqs. (5))
λ_1,λ_2	Bearing fluid circumferential average velocity ratios
$\phi_{i\nu}$	Modal function amplitudes
ψ_1,ψ_2	Bearing fluid film radial stiffness nonlinear functions of journal eccentricities
ω	Complex eigenvalue, also frequency of rotor self-excited vibrations
ω_n	Natural frequency
Ω	Rotative speed
Ω_{st}	Stability threshold

INTRODUCTION

Dynamic phenomena induced by interaction between the rotor and the surrounding fluid, such as occurs in fluid—lubricated bearings and seals of fluid—handling machines have been recognized for over 60 years. Resulting rotor lateral self—excited vibrations are known as "whirl," "whip," or simply "rotor instability." Most of the existing literature documented occurrences of these phenomena in low ranges of rotative speeds (Kirk et al, 1980, Wachel, 1982, Doyle, 1980, Baxter, 1983, Schmied, 1988, Laws, 1985). Classical literature on fluid—lubricated bearings which concentrates on lubrication problems rather than instabilities, reports only occurrences of whirl vibrations of rigid rotors. When the rotating shaft and surrounding fluid involved in motion are considered as one system, it is evident that vibration modes interact. If the whirl or whip vibrations occur at relatively low rotative speed, the shaft would vibrate as either rigid body (whirl), or at its first lateral mode (whip)(Muszynska, 1986a). With the rotative speed increase, there is a smooth transition from the whirl to whip. It is obvious that both these phenomena are generated by the same source. With an increase of rotative speed, higher mode whirl or whip vibrations may be induced (Muszynska, 1988a). Modal approach in rotor system modeling allows for clear interpretation of the occurring vibrational phenomena.

This paper is a continuation of the series of papers (Muszynska, 1986a,b, 1988a,b, 1990, Bently et al., 1988, 1989) on applications of the improved model of the fluid force for lightly loaded shafts rotating in a fluid environment. Following Bolotin (1963) and Black (1969, 1970), the fluid force model is based on the strength of circumferential flow generated mainly by the shaft rotation (Muszynska, 1988c). This model can be used for bearings as well as seals (with or without preswirls and/or injections). The fluid force model identified experimentally by using perturbation techniques (Muszynska, 1986c) allows for more adequate prediction of stability thresholds, and evaluation of the post—stability fluid-induced rotor lateral self—excited limit cycle vibration (whirl and whip) parameters.

In the previous papers (Muszynska, 1986a,b, 1988a,b, Bently, 1988, 1989) the considered rotor models included one and two lateral, isotropic rotor modes, and one source of fluid force in a bearing or a seal. The paper by Muszynska (1990) discussed a case of one mode isotropic rotor supported in two fluid—lubricated bearings, thus containing two sources of potential instability of the rotor. In the present paper the isotropic rotor model includes two lateral modes. The rotor is supported in two fluid—lubricated bearings.

As previously, the modal approach is applied in rotor modeling. The rotor system eigenvalue problem is solved, and approximate values of natural frequencies and thresholds of stability are given. It is shown that there exist fluid—generated natural frequencies of the system and the cor-

Presented at the International Gas Turbine and Aeroengine Congress and Exposition
Orlando, FL June 3-6, 1991

responding modes. The nonlinear model allows for calculation of the after-threshold self–excited vibration parameters of the whirl or whip type.

The most important and new result presented in this paper is the simultaneous existence of the self–excited vibrations corresponding to two lateral modes of the rotor. The results of experiments are given. The model predicts this phenomenon, and provides measures to control it.

MATHEMATICAL MODEL OF A TWO–MODE SHAFT ROTATING IN TWO FLUID–LUBRICATED BEARINGS

Consider a balanced isotropic rotor supported by two fluid 360° lubricated bearings (Fig. 1). The equations of lateral vibrations of the shaft concentrically rotating in the bearings are as follows:

$$\left.\begin{aligned} &M_1\ddot{z}_1 + D_{S1}\dot{z}_1 + K_6 z_1 - K_8 z_2 - K_1 z_3 = 0 \\ &M_2\ddot{z}_2 + D_{S2}\dot{z}_2 + K_7 z_2 - K_8 z_1 - K_4 z_4 = 0 \\ &M_3\ddot{z}_3 + D_1(\dot{z}_3 - j\lambda_1\Omega z_3) + (K_1+K_{B1})z_3 + z_3\psi_1(|z_3|) - K_1 z_1 = 0 \\ &M_4\ddot{z}_4 + D_2(\dot{z}_4 - j\lambda_2\Omega z_4) + (K_4+K_{B2})z_4 + z_4\psi_2(|z_4|) - K_4 z_2 = 0 \end{aligned}\right\} \quad (1)$$

$$z_5 = \frac{K_2 z_1 + K_3 z_2}{K_2+K_3+K_5}, \qquad K_6 = K_1 + \frac{1}{\frac{1}{K_2}+\frac{1}{K_3+K_5}},$$

$$K_7 = K_4 + \frac{1}{\frac{1}{K_3}+\frac{1}{K_2+K_5}}, \qquad K_8 = \frac{1}{\frac{1}{K_2}+\frac{1}{K_3}+\frac{K_5}{K_2 K_3}} \quad (2)$$

$$z_i(t) = x_i(t) + jy_i(t), \quad |z_i| = \sqrt{x_i^2 + y_i^2}, \; i=1,...,4, \quad j=\sqrt{-1} \quad (3)$$

where x_i, y_i are rotor horizontal and vertical displacements, M_i, K_i, i=1,...,4, D_{S1}, D_{S2} are rotor generalized (modal) masses, stiffnesses, and damping coefficients respectively. Note that the rotor model includes two modes. The corresponding modal parameters can be obtained analytically by modal reduction of the finite element model or identified expermentally (Muszynska et al., 1989). In Eqs. (1) K_{B1}, K_{B2}, D_1, D_2 are bearing fluid film radial stiffnesses and radial damping coefficients respectively; λ_1 and λ_2 are circumferential average velocity ratios, as defined by Muszynska, 1988c. With a simplification, λ can be represented by the ratio of the bearing cross stiffness to the product of radial damping and rotative speed. In the classical literature λ is a priori assumed constant and equal to 0.5 (Bolotin 1963, Black 1969, 1970). K_5 is the stiffness of an additional supporting spring, Ω is the rotative speed, ψ_1,ψ_2 are the fluid nonlinear stiffness functions of corresponding radial displacements of the rotor (Muszynska, 1986a). They are assumed here in the very general functional form, thus the results are valid for any type of fluid–lubricated bearings. The rotor lateral displacements are expressed using the complex number formalism. For clarity of presentation, the unbalance forces, cross damping, fluid inertia, and other nonlinear functions are omitted.

EIGENVALUE PROBLEM: NATURAL FREQUENCIES, THRESHOLDS OF STABILITY, AND MODES

The eigenvalue problem for linear Eqs. (1) (i.e., when $\psi_1=\psi_2=0$) provides the following characteristic equation:

$$(\kappa_1\kappa_3 - K_7^2)(\kappa_2\kappa_4 - K_8^2) - K_8^2\kappa_3\kappa_4 = 0 \quad (4)$$

where

$$\kappa_1 = K_6 + jD_{S1}\omega - M_1\omega^2, \quad \kappa_3 = K_1 + K_{B1} + jD_1(\omega - \lambda_1\Omega) - M_3\omega^2$$
$$\kappa_2 = K_7 + jD_{S2}\omega - M_2\omega^2, \quad \kappa_4 = K_4 + K_{B2} + jD_2(\omega - \lambda_2\Omega) - M_4\omega^2 \quad (5)$$

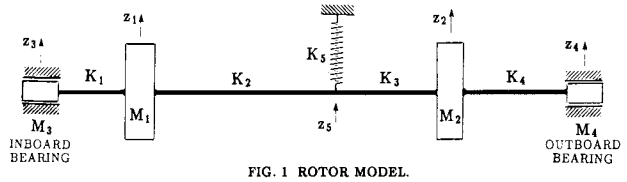

FIG. 1 ROTOR MODEL.

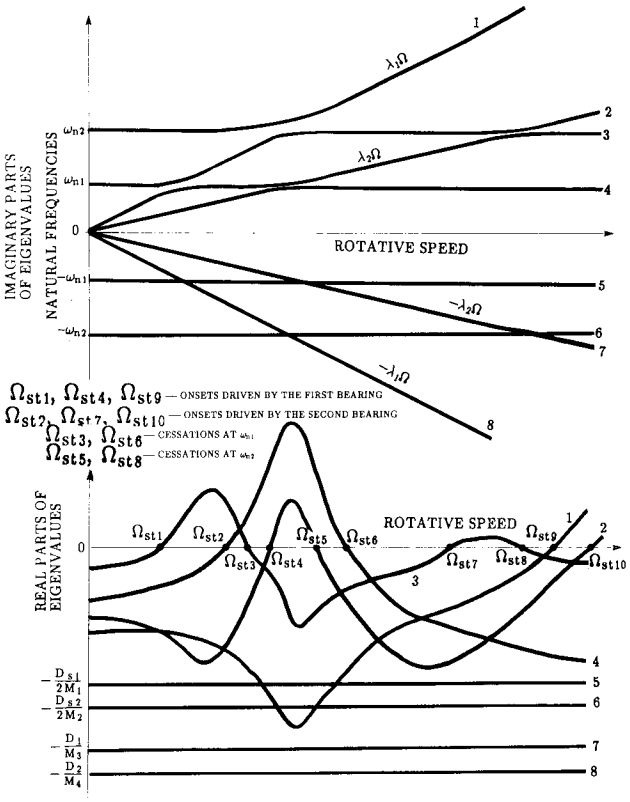

FIG. 2 IMAGINARY AND REAL PARTS OF THE EIGENVALUES s = jω.

are system dynamic stiffnesses and ω is a complex eigenvalue.

Parametric analysis of Eq. (4) using the coefficient values in the range identified from real systems yields the generalized results regarding the system natural frequencies and thresholds of stability. They are qualitatively summarized in Fig. 2. Two natural frequencies are close to the values $\lambda_1\Omega$ and $\lambda_2\Omega$, thus are due to the bearing fluid circumferential flow ("whirl" frequencies, Muszynska, 1986a). The corresponding real parts of these eigenvalues s=jω have negative and positive values, so they provide the important thresholds of stability (onsets). The next two eigenvalues are close to

$$s = -(D_1/M_3) - j\lambda_1\Omega, \qquad s = -(D_2/M_4) - j\lambda_2\Omega, \quad (6)$$

and their constant negative real parts assure stability.

The remaining four eigenvalues s have imaginary parts close to the two-mode rotor natural frequencies ("whip" frequencies, Muszynska 1986a):

$$\omega_{n1,2,3,4} \approx \pm\left\{\frac{K_6}{2M_1}+\frac{K_7}{2M_2} \pm \sqrt{\left[\frac{K_6}{2M_1}-\frac{K_7}{2M_2}\right]^2 + \frac{K_8^2}{M_1 M_2}}\right\}^{1/2} \quad (7)$$

The real parts corresponding to the negative frequencies (7) are negative, approaching the values $-D_{S1}/2M_1$, $-D_{S2}/2M_2$ respectively, so they assure stability of the system. The real parts corresponding to the positive natural frequencies (7) may be negative or positive, thus provide additional thresholds of stability (cessations). All thresholds of stability depend directly on the bearing fluid circumferential average velocity ratios. They are inverse proportional to either λ_1 or λ_2, or a combination of both.

Following the results of Muszynska, 1990, the approximate values of the first mode whirl instability onsets driven by the first and second bearings are respectively:

$$\Omega_{st1} \approx \frac{\omega_{n1}}{\lambda_1}\sqrt{1 - \frac{1}{2\left[1+\frac{K_{B1}-M_3\omega_{n1}^2}{K_{m1}}\right]}}, \quad (8)$$

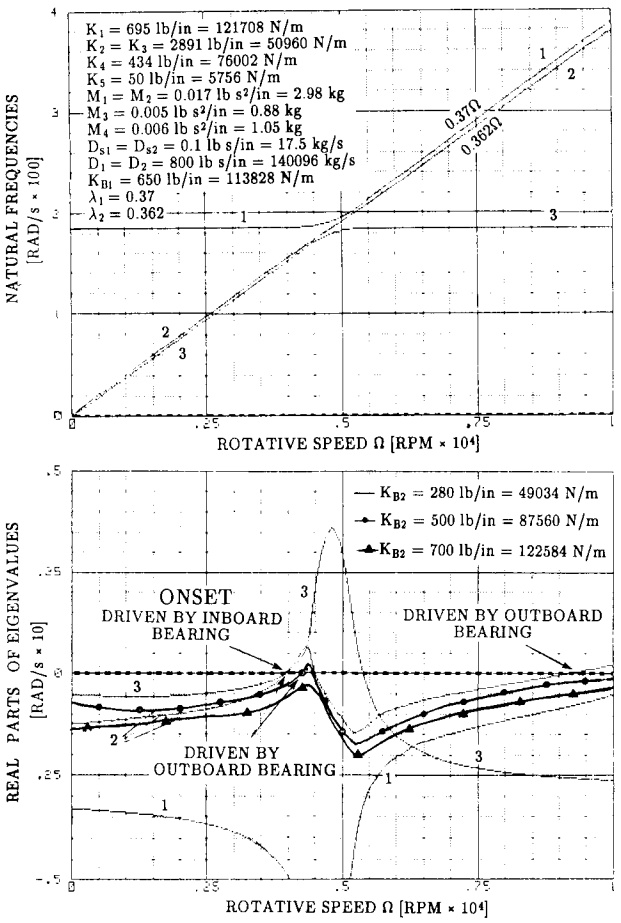

FIG. 3 ROTOR SYSTEM EIGENVALUES FOR PARTICULAR CASES. NOTE CHANGES IN STABILITY THRESHOLDS WITH INCREASE OF THE OUTBOARD BEARING FLUID FILM RADIAL STIFFNESS. THE OTHER REAL AND IMAGINARY PARTS OF EIGENVALUES ARE PRACTICALLY INSENSITIVE TO K_{B2}. WITH AN INCREASE OF K_{B2}, BOTH ONSETS OF INSTABILITY DRIVEN BY THE OUTBOARD BEARING OCCUR AT HIGHER ROTATIVE SPEEDS. FOR SUFFICIENTLY HIGH K_{B2}, ONLY THE SECOND INSTABILITY EXISTS.

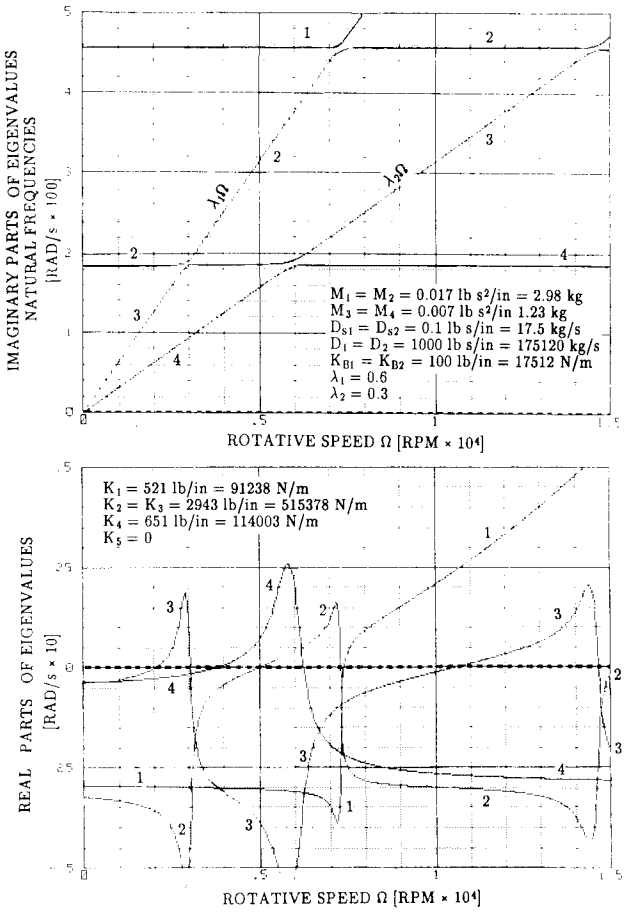

FIG. 4 ROTOR SYSTEM EIGENVALUES FOR A PARTICULAR CASE.

$$\Omega_{st2} \approx \frac{\omega_{n1}}{\lambda_2}\sqrt{1-\frac{1}{2\left[1+\frac{K_{B2}-M_4\omega_{n1}^2}{K_{m1}}\right]}}$$

where ω_{n1} is the rotor first mode positive natural frequency (7) and K_{m1} is the corresponding rotor first mode modal stiffness. The role of the fluid circumferential velocity ratios and fluid film radial stiffnesses in the rotor stability are evident: A decrease of λ_1,λ_2 and/or increase of K_{B1}, K_{B2} cause an increase of the stability onsets. For sufficiently high radial stiffness K_{B2}, this first mode whirl instability onset will not occur (see Fig. 3). With another step of approximation, the similar formulas as Eqs. (8), with ω_{n2} and K_{m2}, respectively, correspond to the second mode whirl instability onsets.

Some numerical examples are given in Figs. 3 and 4. It can be noticed that for relatively high values of the fluid damping D_1,D_2, the coupling of the system causes the cross sections of the positive constant and rotative speed-dependent natural frequencies to degenerate into hyperbolas. This effect does not take place for negative frequencies.

The modal functions $\bar{\phi}_{i\nu} = z_i/z_\nu$ of the linear system (1) can be defined as complex displacement ratios related to the first disk (ν=1). They represent complex numbers as follows:

$$\bar{\phi}_{21} \equiv \phi_{21}e^{j\beta_{21}} = \frac{\kappa_4}{K_4^2K_8}\left[(\kappa_1\kappa_2-K_8^2)-K_1^2\frac{\kappa_2}{\kappa_3}\right] \equiv \frac{1}{K_8}(\kappa_1-K_1^2/\kappa_3)\,, \quad (9)$$

$$\bar{\phi}_{31} \equiv \phi_{31}e^{j\beta_{31}} = \frac{K_1}{\kappa_3}\,, \quad (10)$$

$$\bar{\phi}_{41} = \bar{\phi}_{42}\bar{\phi}_{21} = \phi_{41}e^{j\beta_{41}} = \phi_{42}\phi_{21}e^{j(\beta_{42}+\beta_{21})} = \frac{K_4}{\kappa_4}\phi_{21}e^{j\beta_{21}}\,, \quad (11)$$

where the modal function amplitudes $\phi_{i\nu}$ and phases $\beta_{i\nu}$ can easily be calculated from Eqs. (5) for the corresponding eigenvalues ω obtained from Eq. (4). The rotor modes at "whip" frequencies (7) are classical. The rotor disks vibrate in phase for the lower natural frequency and 180° out of phase for the higher one. Interesting are modal function phase angles of the inboard journal relative to the first disk (β_{31}), and the outboard journal relative to the second disk (β_{42}):

$$\beta_{31} = \arctan\frac{D_1(\lambda_1\Omega-\omega)}{K_1+K_{B1}-M_3\omega^2} \quad (12)$$

$$\beta_{42} = \arctan\frac{D_2(\lambda_2\Omega-\omega)}{K_4+K_{B2}-M_4\omega^2} \quad (13)$$

For the whirl driven by the inboard bearing $\omega \approx \lambda_1\Omega$, thus β_{31} equals either zero or 180°, depending on whether $\Omega < \frac{1}{\lambda_1}\sqrt{\frac{K_1+K_{B1}}{M_3}}$ or $\Omega > \frac{1}{\lambda_1}\sqrt{\frac{K_1+K_{B1}}{M_3}}$. This means that for the lower mode whirl vibrations, the journal and the first disk vibrate in phase; for the higher modes, they are out of phase. The similar reasoning holds true in case of the second disk and outboard journal phase, when the whirl is driven by the outboard bearing (Eq. (13)).

If the whirl is driven by the inboard bearing, and $\lambda_1 > \lambda_2$, then β_{42} falls either between 270° and 360° when $\Omega < \frac{1}{\lambda_2}\sqrt{\frac{K_4+K_{B2}}{M_4}}$, or between 180° and 270° if $\Omega > \frac{1}{\lambda_2}\sqrt{\frac{K_4+K_{B2}}{M_4}}$, approaching 180° when the

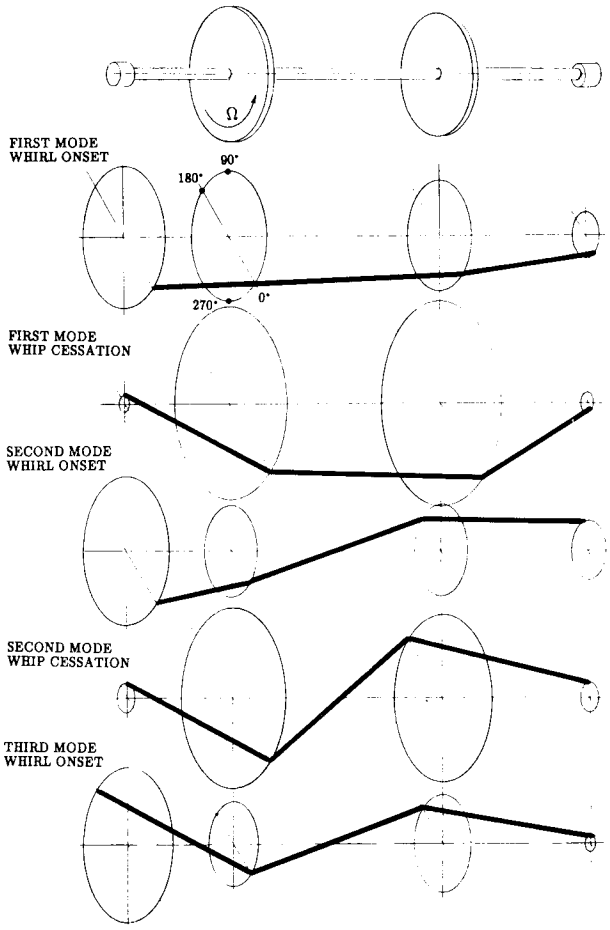

FIG. 5 ROTOR MODES AT THRESHOLDS OF STABILITY. THREE MODES DRIVEN BY THE OUTBOARD BEARING ARE NOT DISPLAYED.

speed Ω increases. If $\lambda_1 < \lambda_2$, then either $0° < \beta_{42} < 90°$ for the respective lower speed range, or $90° < \beta_{42} < 180°$ for the higher range, also approaching 180° with the speed increase. At the whip cessations, β_{31} and β_{42} are close to 90° or 270°. Note that all modes are three dimensional.

The summary of rotor modes at instability thresholds driven by the inboard bearing is presented in Figure 5. The classical rotor modes are labeled "whip" modes. In the most unstable case there exist two whip and six whirl modes; the latter are driven by each bearing separately.

SYMMETRIC CASE

In case of axial symmetry, i.e. when $M_1=M_2$, $M_3=M_4$, $K_6=K_7$, $K_1=K_4$, $K_{B1}=K_{B2}$, $D_{S1}=D_{S2}$, $D_1=D_2$, $\lambda_1=\lambda_2$, the linear system dynamic stiffnesses are equal respectively, $\kappa_1=\kappa_2$, $\kappa_3=\kappa_4$. The characteristic equation (4) reduces to the following form:

$$(\kappa_1\kappa_3 - K_1^2)^2 - K_8^2\kappa_3^2 = 0$$

which can be simplified, as follows:

$$\kappa_3(\kappa_1 \pm K_8) - K_1^2 = 0 \qquad (14)$$

Eq. (14) is of the same format, as discussed by Muszynska, 1986a, except that the expression $\kappa_1 \pm K_8$ describes now two modes of the rotor, with two natural frequencies $\omega_n = \pm\sqrt{(K_6 \pm K_8)/M_1}$ ("whip" frequencies). Following the results of Muszynska, 1986a and 1988a, the four onsets of whirl instability occur approximately at the following rotative speeds:

$$\Omega_{st1,4,4,9} \approx \frac{1}{\lambda_1}\left[\frac{K_6 \pm K_8}{2M_1} + \frac{K_1+K_{B1}}{2M_3} \pm \right.$$

$$\left. \pm \sqrt{\left[\frac{K_6 \pm K_8}{2M_1} - \frac{K_1+K_{B1}}{2M_3}\right]^2 + \frac{K_1^2}{M_1 M_3}}\right]^{\frac{1}{2}}$$

Note that the instability onsets practically do not depend on damping. Two approximate values for the middle onset "4" are given. They differ by the level of approximation.

The cessations of instability for the first and the second mode "whips" occur approximately at the following rotative speeds:

$$\Omega_{st3,5} \approx \frac{\omega_{n1,2}}{\lambda_1}\left[1 + \frac{K_1^2}{D_1 D_{S1}\,\omega_{n1,2}}\right] \qquad (15)$$

The role of both shaft and fluid dampings is evident here: the higher their values, the lower rotative speed at which rotor becomes stable again. If $\Omega_{st3}<\Omega_{st1}$ or $\Omega_{st5}<\Omega_{st4}$, then the corresponding instability modes will not occur at all (see Fig. 3).

SELF–EXCITED VIBRATIONS

The nonlinear Eqs. (1) have exact periodic solutions

$$z_1 = A_1 e^{j(\omega t+\alpha_1)}, \qquad z_3 = A_3 e^{j(\omega t+\alpha_3)},$$
$$z_2 = A_2 e^{j(\omega t+\alpha_2)}, \qquad z_4 = A_4 e^{j\omega t} \qquad (16)$$

with frequency (or frequencies) ω, amplitudes A_1, A_2, A_3, A_4 and phases α_1, α_2, α_3 relative to the phase $\alpha_4=0$ of the outboard bearing journal. Eqs. (16) describe the rotor lateral self–excited vibrations, known as whirl and whip. They occur as limit cycles after the onsets of instability.

The frequencies, amplitudes, and phases of Eqs. (16) can be calculated from the set of nonlinear algebraic equations obtained by substituting (16) into Eqs. (1), and dividing all terms by $e^{j\omega t}$:

$$\kappa_1 A_1 e^{j\alpha_1} - K_8 A_2 e^{j\alpha_2} - K_1 A_3 e^{j\alpha_3} = 0, \quad [\kappa_3 + \psi_1(A_3)]A_3 e^{j\alpha_3} - K_1 A_1 e^{j\alpha_1} = 0$$
$$\kappa_2 A_2 e^{j\alpha_2} - K_8 A_1 e^{j\alpha_1} - K_4 A_4 = 0, \quad [\kappa_4 + \psi_2(A_4)]A_4 - K_4 A_2 e^{j\alpha_2} = 0 \qquad (17)$$

Note that with assumed solution (16) the arguments of the nonlinear functions become equal to the corresponding vibration amplitudes. Similarly to the results obtained for other rotor systems (Muszynska, 1986a, 1988a), it is concluded here that the frequencies calculated from Eqs. (17) are numerically very close to the natural frequencies of the linear equations (1) at thresholds of stability. The amplitudes A_3 and A_4 of the journal self-excited vibrations depend on the nonlinear characteristics of the functions $\psi_1(A_3)$ and $\psi_2(A_4)$. The self–excited limit cycle vibration amplitudes and phases of the rotor disks, calculated from Eqs. (17), are as follows:

$$A_1 e^{j\alpha_1} = \frac{K_4 K_8 A_4 + \kappa_2 K_1 A_3 e^{j\alpha_3}}{\kappa_1\kappa_2 - K_8^2}, \quad A_2 e^{j\alpha_2} = \frac{K_1 K_8 A_3 + \kappa_1 K_4 A_4}{\kappa_1\kappa_2 - K_8^2}. \qquad (18)$$

The vibrations at the journals act as exciting forces transmitted to the disks. The disk responses depend on the amount of this excitation, and on the rotor dynamic stiffness characteristics, as well. The expression standing in the denominators of Eqs. (18), when equalized to zero, represents the two–mode rotor characteristic equation, yielding the natural frequencies (7). Thus, it is clear that when the self–excited vibration frequency is close to any of the values (7), the amplitudes A_1 and A_2 become high. These self–excited vibrations are known as "whip." The other self–excited vibration frequencies are close to the values $\lambda_1\Omega$ and $\lambda_2\Omega$, and the self–excited vibrations are known as "whirl." The whirl and whip vibrations can be driven by either inboard or outboard bearing fluid forces. It is possible that several self-excited vibrations with different frequencies, and corresponding to different modes, occur at the same time. This event was confirmed by experimental data, described later in this paper.

Note that the phase angle $(\alpha_3-\alpha_1)$ corresponds to the angle β_{31}, and α_2 corresponds to β_{42} discussed previously. The only difference in comparison to Eqs. (12) and (13) is the addition of $\psi_1(A_3)$ to K_{B1} and $\psi_2(A_4)$ to K_{B2}. This suggests that the free modes will only slightly differ from the shaft deflection lines during the self–excited vibrations.

RADIAL PRELOAD EFFECT

A constant radial force applied to the rotor results mainly in static displacement of the journals to eccentric positions inside the bearings (some slight increase of the rotor stiffness can also take place). The journal eccentric rotation results in fluid film radial stiffness and damping increase, and a reduction of the circumferential velocity ratios (Muszynska 1986b, 1988c) in a specific radial direction of the rotor static displacement. The rotor characteristics become anisotropic.

In a rough approximation, the preloaded system can still be modeled by Eqs. (1), with higher values of D_1, D_2, K_{B1}, and K_{B2}, and lower λ_1, λ_2 than for the concentric rotor. The latter four parameters have significant influence on the stability threshold increase. The effect of fluid stiffness increase is shown on the numerical example illustrated in Figure 3. A reduction of the fluid circumferential velocity ratio causes an increase of the instability onsets. An increase of the fluid radial damping moves the cessation thresholds down to the lower rotative speed range.

In summary, the rotor eccentricity due to the external radial preload, causing changes in the fluid forces, results in the well—known rotor stabilization, discussed widely in the literature. This effect is illustrated by the following experimental data.

EXPERIMENTAL RESULTS

The test rotor rig was built to demonstrate destabilizing effects of fluid dynamic forces in the two oil—lubricated bearing rotor system (Fig. 6). A flexible two—mass well—balanced shaft is supported at each end by circular 360° lubricated bearings. The lubricant is T—10 oil. Each bearing of 0.7" (1.78×10^{-2}m) length and 6 mil (152×10^{-6}m) radial clearance has four equally spaced, radial inlet ports entering at the center of four "canoe" shaped symmetric axial grooves. Each groove is 24 mil (6.1×10^{-4}m) deep at the center and has a total axial length of 0.5" (12.7×10^{-3}m). This allows for even fluid pressure around the journal. The ports are connected to one oil pressure regulator. The pressure in each bearing can be controlled separately. In this experiment the oil pressure in both bearings was maintained constant at 3 psi (20683 N/m^2). The oil temperature (affecting viscosity) was also maintained constant, and monitored using a thermocouple that was located in the drain tube of the outboard bearing.

The rotational energy is derived from a 0.5 hp electric motor which is connected to the rotor through a flexible coupling. A speed controller was used to control rotative speed and acceleration. Supporting orthogonal springs at each end of the rotor and at its midspan allow balancing the force of gravity, and may provide radial preload forces on the shaft. The shaft equilibrium can be obtained at any eccentric shaft position in the bearing. To obtain the shaft lateral vibration data, the eddy current displacement probes were mounted at both ends of the shaft in an XY configuration. An optical Keyphasor® was used to provide angular orientation, rotative speed, and/or timing information. A computerized data acquisition and processing system was used.

The results of start—up responses of the concentric rotor and the eccentric rotor with four radial preload cases are presented in Table 1 and in the form of spectrum cascade plots (Figures 7 to 11).

On the concentrically rotating rotor, the first onset of stability occurs at ~4000 rpm (Fig. 7). At this speed the self—excited limit cycle vibrations are clearly visible in the spectrum. With the first natural (first balance resonance) frequency $\omega_{n1} \approx 1769$ rpm, the fluid velocity ratio λ_1 calculated from the first part of Eq. (8) must be lower than 0.44. Since the instability occurs in the transition range from the whirl to whip frequency, at higher rotative speeds only the whip vibrations exist. At the rotative speed ~8700 rpm, the second mode whirl occurs. The whirl—to—rotative— speed ratio at this instability onset is 0.48, thus the fluid velocity ratio must then be lower than 0.48. Changes in the frequency of vibration with the rotative speed increase are characteristic for the whirl. Soon, however, the second mode whirl transforms into the second mode whip, and its frequency approaches the second natural frequency of 4309 rpm. At high rotative speeds the rotor vibrations are very violent, especially near mid—span locations. The whip vibrations measured at the inboard and outboard locations were filtered using a vector filter manually tuned to respective whip frequencies. The phases of vibration obtained by further signal processing indicate that at the first mode whip, both shaft ends vibrate almost in phase; however, the shaft outboard end lags the inboard end by about 2 degrees. This indicates that this mode is driven by the inboard bearing. In the second mode whip the average phase lag of the shaft inboard versus outboard ends is about 182 degrees. This means that this mode has been driven by the outboard bearing.

The rotor system was modeled, using Eqs. (1), and the eigenvalues are presented in Figure 3. The rotor modal parameters have been identified using the method described in the paper by Muszynska et al. (1989); note the natural frequencies matching the experimental results (Fig. 7). With estimated (not fully identified) fluid force parameters, the calculated first instability onset driven by both bearings occurs at 3962 rpm, the second mode onset at 9156 rpm (Fig. 3), thus is slightly higher than the one observed in the experiment. The parametric sensitivity test of the eigenvalues reveals that the second mode whip is driven by the outboard bearing. An increase of the outboard fluid film stiffness moves the stability onsets to higher rotative speed range. The model predicts it, and the further experiments with preload cases confirm this effect. Some discrepancies between analytical and experimental results are due to the fact that when the second mode whirl then whip occur, the experimental rotor is already at the first mode whip conditions. This means that the fluid film radial stiffnesses and circumferential velocity ratios are different than before the first onset of instability. For a more adequate calculation of the second mode instability onset, the rotor model parameters should then be slightly modified. The linear model indicates that there exist cessations of instability for the whip vibrations of both modes of the rotor. These cessation speeds correspond, however, to the original parameters of the rotor, while, actually, the rotor is already at the whip conditions. The stability of rotor zero lateral vibrations predicted by the linear model differs from the stability of whirl/whip vibrations (Muszynska, 1988b).

The figures 8 to 11 illustrate the rotor behavior when the radial preload was applied. The preloading of the outboard side of the rotor does not affect the first mode whip; it stabilizes, however, the second mode whirl/whip in the considered range of rotative speeds (Fig. 8; compare with positions of stability thresholds illustrated in Fig. 3 for several values of the outboard bearing fluid film radial stiffness). The preloading of the rotor inboard side revealed that the inboard bearing fluid was the main driving factor of the lower instability onset. The first mode whip still occurs, but its onset is at higher speed (λ_1<0.38, Fig. 9), and the vibration amplitudes are smaller.

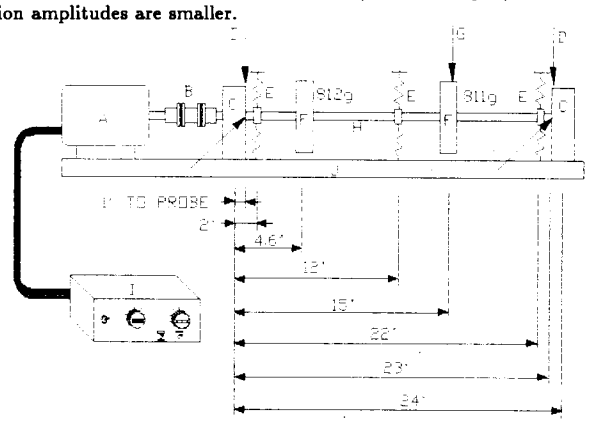

A — 0.5 HP AC MOTOR
B — FLEXIBLE THOMAS COUPLING, MODEL CB25
C — 360° OIL LUBRICATED BEARING, L/D=0.75
D — XY EDDY CURRENT DISPLACEMENT PROBES
E — SPRING SUPPORT, STIFFNESS 50 LB/IN
F — CIRCULAR DISK
G — OPTICAL KEYPHASOR PROBE
H — .375" DIAMETER SHAFT
I — SPEED CONTROLLER
J — ROTOR BASE

FIG. 6 EXPERIMENTAL ROTOR RIG.

Table 1. Resonant Frequencies and Thresholds of Stability of the Experimental Rotor

Case		1	2	3	4	5
Figure Number		7	8	9	10	11
Preload [lb]/[degree]	Inboard	0	0	55.5/315°	23.62/270°	32.3/315°
	Outboard	0	55.5/315°	0	23.62/90°	32.3/315°
Rotor Displacement [mils]	Inboard Vertical	0	0.12	8.12	0.86	6.84
	Inboard Horizontal	0	0.13	10.01	8.67	8.79
	Outboard Vertical	0	8.85	0.12	0.67	7.63
	Outboard Horizontal	0	10.99	0.55	9.28	10.56
Resonant Frequency [rpm]	First Mode	1769	1827	1890	1798	1950
	Second Mode	4309	4408	4410	4309	4365
Stability Threshold [rpm]	First Mode	4000	4000	5000	8000	Above 1000
	Second Mode	8700	Above 9600 rpm			
Predicted Stability Threshold [rpm] (Fig. 3)	First Mode	(K_{B2}=280) 3962	(K_{B2}=500 lb/in) 3947*			
	Second Mode	9156	10182			

*Calculated by using isotropic model (Fig. 3). Agreement qualitative only.

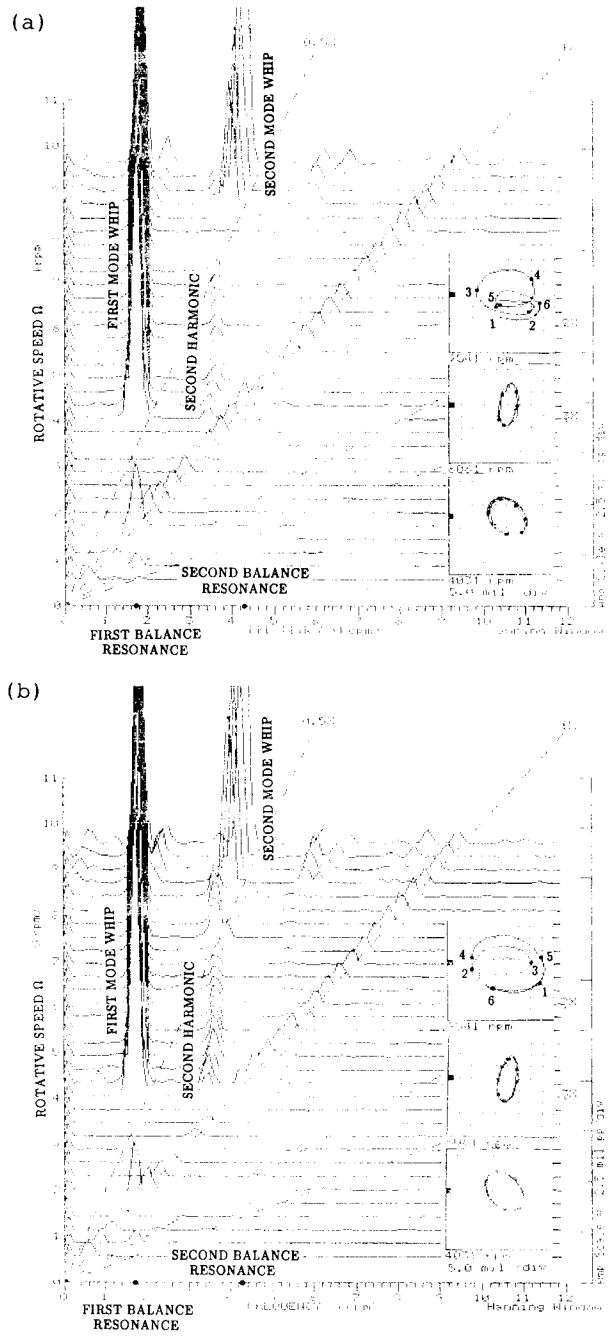

FIG. 7 SPECTRUM CASCADE OF THE START-UP AND SELECTED ORBITS OF THE INBOARD (a) AND OUTBOARD (b) VERTICAL RESPONSES OF THE CONCENTRIC ROTOR (CASE 1). THE SELF-EXCITED LIMIT CYCLE VIBRATIONS ARE PRESENT IN THE SPECTRUM. THE NUMBERS AT THE ORBITS INDICATE THE CORRESPONDING TIME MOMENTS OF CONSECUTIVE ROTATIONS. THE INTERNAL LOOPS AT OPPOSITE SIDES ON THE INBOARD AND OUTBOARD ORBITS AT 9541 rpm INDICATE 180° OUT OF PHASE OF THE SECOND MODE WHIP. BOTH MODE WHIPS ARE FORWARD.

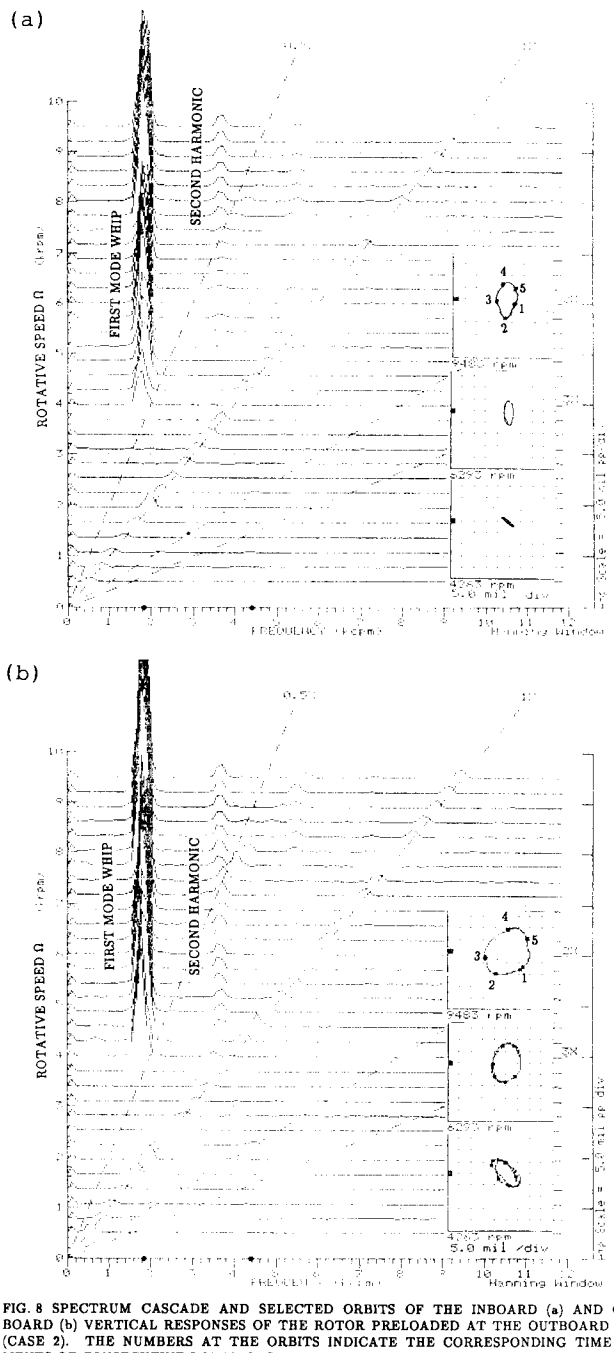

FIG. 8 SPECTRUM CASCADE AND SELECTED ORBITS OF THE INBOARD (a) AND OUTBOARD (b) VERTICAL RESPONSES OF THE ROTOR PRELOADED AT THE OUTBOARD SIDE (CASE 2). THE NUMBERS AT THE ORBITS INDICATE THE CORRESPONDING TIME MOMENTS OF CONSECUTIVE ROTATIONS.

The preload applied at both rotor ends moves further up the instability onset (now λ_1 and λ_2 must be lower than 0.22, Fig. 10). Further increase of the preload force stabilizes the rotor in the considered range of rotative speeds (Fig. 11).

Note that the preload conditions slightly modify the natural frequencies of the rotor (the first and second balance resonance frequencies slightly differ for the considered cases; see Table 1). The preload also results in some changes in the rotor balance state. The synchronous (1×) vibration response amplitudes differ from case to case, which is especially evident at the balance resonance speeds.

FINAL REMARKS

A further application of the lightly loaded bearing fluid force models in rotordynamics is presented in this paper. The modal approach in rotor modeling provides easy interpretable results which are adequate to experimental observations of rotor dynamic behavior. In particular, the model predicts the existence of several mode instabilities, and an experimental case exhibiting this phenomenon was documented in this paper. The linear models predict quite well the instability thresholds. The first stability onsets obtained here do not differ much from the onsets calculated by using classical bearing coefficients. The nonlinear model discussed here yields the after–stability onset self–excited vibration parameters, which can be calculated, provided that the nonlinear functions were adequately

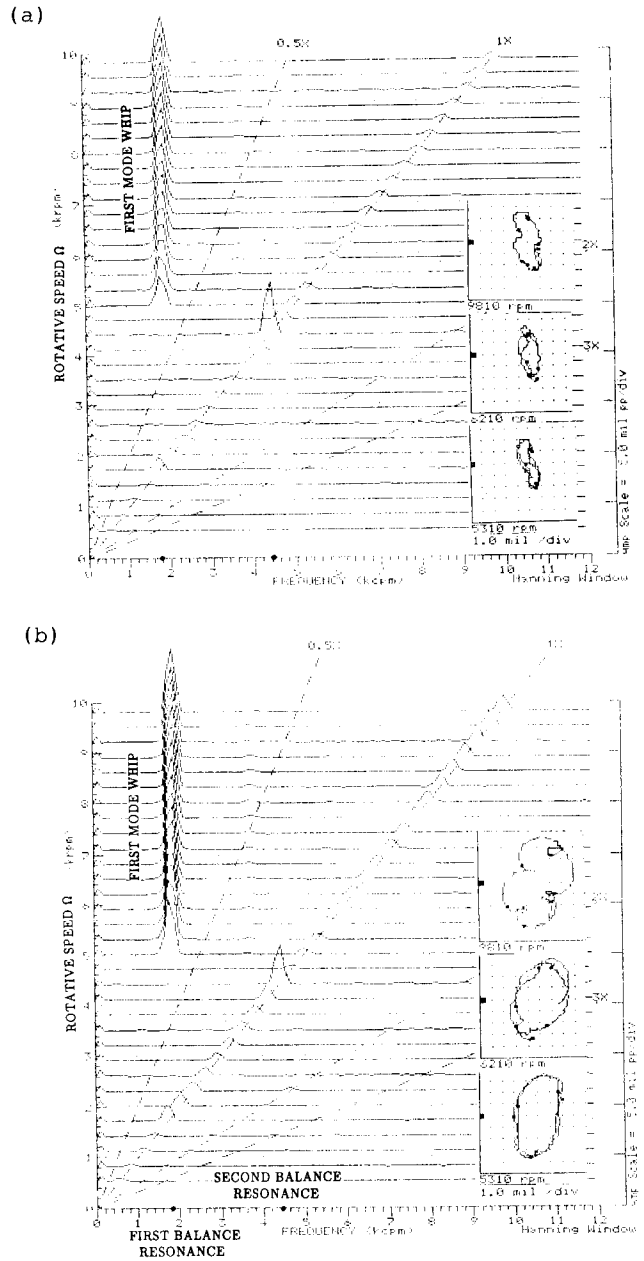

FIG. 9 SPECTRUM CASCADE AND SELECTED ORBITS OF THE INBOARD (a) AND OUTBOARD (b) VERTICAL RESPONSES OF THE ROTOR PRELOADED AT THE INBOARD SIDE (CASE 3).

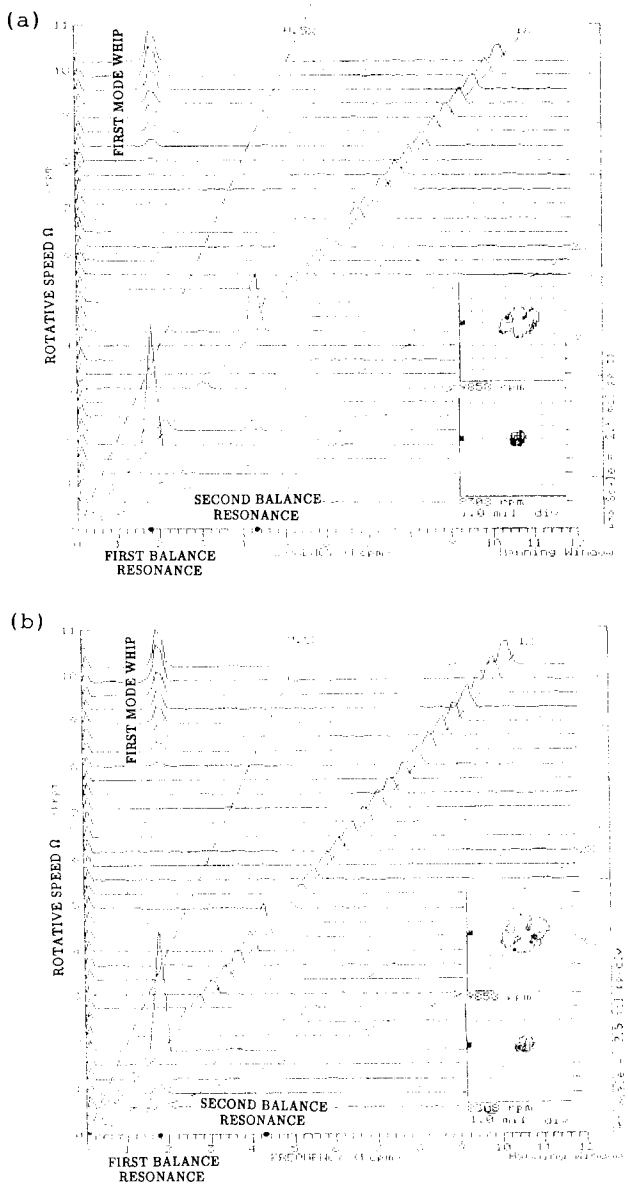

FIG. 10 SPECTRUM CASCADE AND SELECTED ORBITS OF THE INBOARD (a) AND OUTBOARD (b) VERTICAL RESPONSES OF THE ROTOR LIGHTLY PRELOADED AT BOTH INBOARD AND OUTBOARD ENDS (CASE 4).

identified. In this presentation these functions are assumed in a very general form, thus the considerations and results are applicable to any type of fluid-lubricated bearings.

The stability of the self–excited vibrations was not discussed in this paper. It can further be done, following the method discussed by Muszynska 1988b. The experimental results presented here and in the papers by Muszynska (1988, 1990) show that the first mode whip vibrations can exist (means they are stable) in a wide rotative speed range. They may also become unstable (means the rotor stabilizes) in certain ranges. A slight decrease in whip vibration amplitudes in some rotative speed regions was noticed during the present experiments (see in Fig. 7 a decrease of the whip harmonic amplitudes around 7000 rpm). This indicates that some changes in the system parameters did take place. The model predicts that the real parts of the system eigenvalues decrease around this range of the rotative speeds.

The full identification of the experimental system parameters was not performed; only the two–mode modal identification of the rotor itself by using the procedure described by Muszynska et al. (1989) yielded the basic values M_1, M_2 and K_1 to K_5 (Fig. 3). Further identification of the fluid film characteristics will provide better quantitative adequacy of the model. In the qualitative sense, the model is, however, fully adequate to the observable phenomena, and serves better than the classical models of fluid forces in lightly loaded fluid–lubricated bearings.

The ability of theoretical prediction and the experimental evidence of the simultaneous existence of the first and second mode whip vibrations confirm the adequacy and usefulness of the fluid force model, and provides a significant tool to the rotating machinery designers and users. The parametric sensitivity tests on the fluid force model reveal directly which parameters are responsible for instability, thus which ones have to be controlled. These parameters are the fluid film radial stiffness and the fluid circumferential average velocity ratio. For better stability, the first one should be the highest. The increase of this stiffness is possible by increasing the shaft eccentricity inside the bearing and/or by an increase of fluid

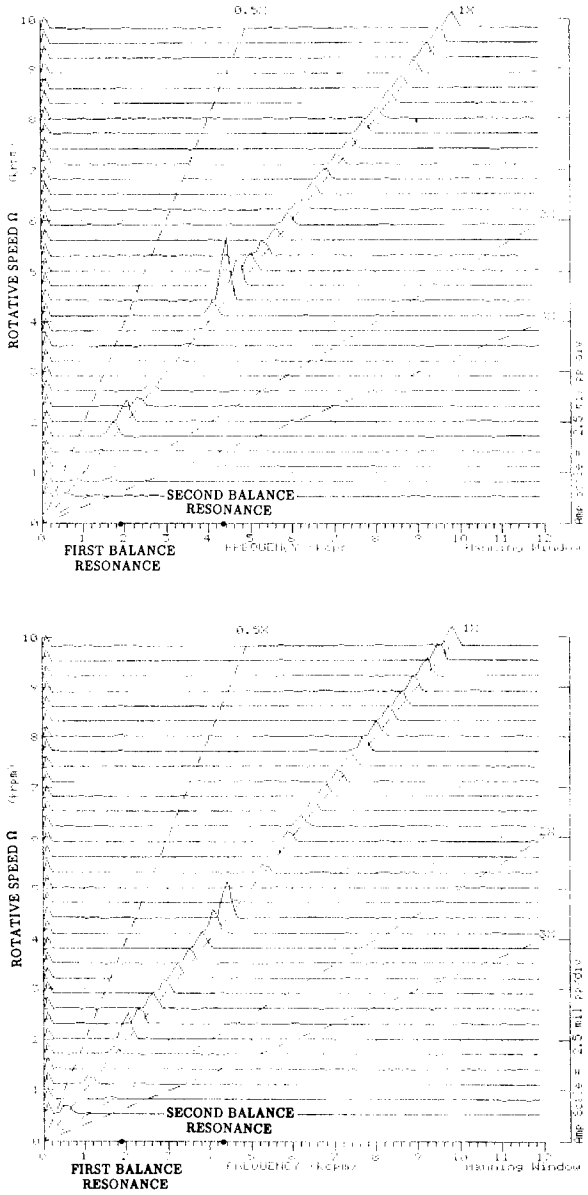

FIG. 11 SPECTRUM CASCADE OF THE INBOARD (a) AND OUTBOARD (b) VERTICAL RESPONSES OF THE ROTOR MORE HEAVILY PRELOADED AT BOTH INBOARD AND OUTBOARD ENDS (CASE 5).

pressure (for 360° lubricated bearings). The fluid circumferential velocity decreases at higher shaft eccentricity, and additionally can effectively be reduced by anti–swirl injections (Bently, 1989).

REFERENCES

Baxter, N. L., 1983, "Case Studies of Rotor Instability in the Utility Industry," Rotor Dynamical Instability, AMD, v. 55, New York.

Bently, D. E. and Muszynska, A., 1988, "Role of Circumferential Flow in the Stability of Fluid–Handling Machine Rotors," Rotordynamics Instability Problems in High Performance Turbomachinery, NASA CP 3026, College Station, Texas, pp. 415–430.

Bently, D. E. and Muszynska, A., 1989, "Anti–Swirl Arrangements Prevent Rotor/Seal Instability," Transactions of the ASME Journal of Vibration, Acoustics, Stress and Reliability in Design, v. 111, No. 2, pp. 156–162.

Black, H. F., 1969, "Effects of Hydraulic Forces in Annular Pressure Seals on the Vibrations of Centrifugal Pump Rotors," Journal of Mechanical Engineering Science, v. II, No. 2.

Black, H. F., Jensen, D. N., 1990, "Dynamic Hybrid Bearing Characteristics of Annular Controlled Leakage Seals," Proceedings Journal of Mechanical Engineering, v. 184.

Bolotin, V. V., 1963, "Nonconservative Problems in the Theory of Elastic Stability," The Macmillan Company, New York.

Doyle, H. E., 1980, "Field Experiences with Rotor Dynamic Instability in High Performance Turbomachinery," Rotordynamic Instability Problems in High–Performance Turbomachinery, NASA CP 2133, College Station, Texas, pp. 3–13.

Kirk, R. G., Nicholas, J. C., Donald, G. H., and Murphy, R. C., 1980, "Analysis and Identification of Synchronous Vibration for a High Pressure Parallel Flow Centrifugal Compressor," Rotordynamic Instability Problems in High Performance Turbomachinery, NASA CP 2133, College Station, Texas, pp. 45–63.

Laws, C. W., 1985, "Turbine Instabilities–Case Histories," Instability in Rotating Machinery, NASA CP 2409, Carson City, Nevada, pp. 65–81.

Muszynska, A., 1986a, "Whirl and Whip — Rotor/Bearing Stability Problems," Journal of Sound and Vibration, v. 110, No. 3, pp. 443–462.

Muszynska, A., 1986b, "Fluid–Related Rotor/Bearing/Seal Instability Problems," Bently Rotor Dynamics Research Corporation, Report No. 2/86, Minden, Nevada, pp. 1–113.

Muszynska, A., 1986c, "Modal Testing of Rotor/Bearing Systems," The International Journal of Analytical and Experimental Modal Analysis, v. 1, No. 3, pp. 15–34.

Muszynska, A., 1988a, "Multi–Mode Whirl and Whip in Rotor/Bearing Systems," Dynamics of Rotating Machinery, Proceedings of the Second International Symposium on Transport Phenomena, Dynamics, and Design of Rotating Machinery, v. 2, Hemisphere Publishing Corporation, Honolulu, Hawaii, pp. 326–340.

Muszynska, A., 1988b, "Stability of Whirl and Whip in Rotor/Bearing Systems," Journal of Sound and Vibration, v. 127, No. 1, pp. 49–64.

Muszynska, A., 1988c, "Improvements in Lightly Loaded Rotor/Bearing and Rotor/Seal Models," Transactions of the ASME, Journal of Vibration, Acoustics, Stress, and Reliability in Design, v. 110, No. 2, pp. 129–136.

Muszynska, A., Bently, D. E., Franklin, W. D., and Hayashida, R. D., 1989, "Identification of Modal Parameters of Rotating Systems Using Perturbation Techniques," Rotating Machinery Dynamics, Proceedings of the Twelfth Biennial ASME Conference on Mechanical Vibration and Noise, Montreal, Canada, DE–v. 18–1, pp. 107-118.

Muszynska, A., 1990, "The Role of Flow–Related Tangential Forces in Rotor/Bearing Seal System Stability," The Third International Symposium on Transport Phenomena and Dynamics of Rotating Machinery (ISROMAC–3), Honolulu, Hawaii.

Schmied, J., 1988, "Rotordynamic Stability Problems and Solutions in High Pressure Turbocompressors," Rotordynamic Instability Problems in High Performance Turbomachinery, NASA CP 3026, College Station, Texas, pp. 395–413.

Wachel, J. C., 1982, "Rotordynamic Instability Field Problems," Rotordynamic Instability Problems in High Performance Turbomachinery, NASA CP 2250, College Station, Texas, pp. 1–19.